IOPscience iopscience.iop.org

Home Search Collections Journals About Contact us My IOPscience

Formation of gallium arsenide nanostructures in Pyrex glass

This content has been downloaded from IOPscience. Please scroll down to see the full text.

2013 Nanotechnology 24 315301

(http://iopscience.iop.org/0957-4484/24/31/315301)

View the table of contents for this issue, or go to the journal homepage for more

Download details:

IP Address: 130.113.31.51
This content was downloaded on 20/11/2013 at 21:58

Please note that terms and conditions apply.

Nanotechnology **24** (2013) 315301 (8pp) doi:10.1088/0957-4484/24/31/315301

Formation of gallium arsenide nanostructures in Pyrex glass

Matiar M R Howlader, Fangfang Zhang and M Jamal Deen

Department of Electrical and Computer Engineering, McMaster University, 1280 Main Street West, Hamilton, ON L8S 4K1, Canada

E-mail: mrhowlader@ece.mcmaster.ca and jamal@mcmaster.ca

Received 27 January 2013, in final form 21 April 2013
Published 15 July 2013
Online at stacks.iop.org/Nano/24/315301

Abstract

In this paper, we report on a simple, low-cost process to grow GaAs nanostructures of a few nm diameter and ∼50 nm height in Pyrex glass wafers. These nanostructures were grown by sequential plasma activation of GaAs and Pyrex glass surfaces using a low-temperature hybrid plasma bonding technology in air. Raman analyses of the activated surfaces show gallium oxide and arsenic oxide, as well as suppressed non-bridging oxygen with aluminate and boroxol chains in glass. The flow of alkaline ions toward the cathode and the replacement of alkaline ions by Ga and As ions in glass result in the growth of GaAs nanostructures in nanopores/nanoscratches in glass. These nanopores/nanoscratches are believed to be the origin of the growth of the nanostructures. It was found that the length of the GaAs nanostructures may be controlled by an electrostatic force. Cross-sectional observation of the bonded interface using high-resolution transmission electron microscopy confirms the existence of the nanostructures. A possible application of the nanostructures in glass is a filtration system for biomolecules.

(Some figures may appear in colour only in the online journal)

1. Introduction

Glass is a commonly used substrate platform in low-cost fluidic systems due to its high biocompatibility, optical transparency and surface hydrophilicity [1–4]. For these applications, the properties of glass may require modification. In [5], a two-step technique to locally modify the bonding structure of the glass matrix through external energy application followed by thermal annealing was proposed. This technique was then used to make Bragg gratings with features ∼250 nm in size. On the other hand, attaching gallium arsenide (GaAs) based electronic and photonic components to the glass-based systems is attractive for opto-fluidic systems for water filtration, or for sensing and monitoring its properties [6, 7].

Direct attachment of GaAs to glass offers increased opportunities in combining electronic and photonic devices with fluidic components. Direct bonding of GaAs or silicon to glass can be used to create systems which are thermally stable, reliable and of low optical loss [8, 9]. Further, a bonding technique that provides for nanostructure growth in glass would open up new possibilities for integrated opto-fluidic and bio-chemical sensing systems [5, 10, 11]. The controllable growth of GaAs nanostructures in glass would also facilitate the fabrication of highly sensitive nanostructures for the miniaturization of fluidic systems at low cost [4]. Among the varieties of glass substrates, Pyrex glass is an excellent material for the growth of nanostructures because its mobile alkali ions, which are electric field dependent, can be used to assist in the growth.

Current techniques to grow nanostructures on, or in glass, require high temperature processing in dry oxygen, nitrogen or argon [12, 13]. Although there has been a significant amount of research on the growth of Si nanoparticles/nanowires in SiO_2 [12, 13], the growth of GaAs nanostructures in SiO_2 or glass has been less intensely investigated [6, 7]. Nanostructures can also be fabricated on different substrates using nanoimprinting lithography over a limited area after thinning down the bonded materials. In this case, the bonding strength of the interface must be strong enough to withstand chemical–mechanical polishing (CMP). Current semiconductor bonding methods [14, 15] that

 © 2013 IOP Publishing Ltd Printed in the UK & the USA

Table 1. Root mean square (RMS) surface roughness, water contact angles of GaAs and glass wafers for anodic bonding and hybrid plasma bonding with bonding processing parameters.

	Bonding method			
	Anodic bonding		Hybrid plasma bonding	
Specimen	GaAs	Glass	GaAs	Glass
RMS surface roughness (nm)	0.18	0.52	0.13	0.46
Contact angle (deg)	77	29	<2	17.7
Processing parameters				
Plasma treatment			O_2 RIE: 50 W for 15 s at 60 Pa followed by N_2 MW radicals: 2.5 kW for 30 s at 60 Pa.	
Cold rolling pressure (MPa)			0.2	
Bonding temperature (°C)	200		200	
Anodic voltage (kV)	1		1	
External pressure (MPa)	0.07		0.07	
Bonding time (min)	10		10	

overcome CMP enable only layer transfer, and, to the best of our knowledge, no mechanism for the growth of GaAs nanostructures in glass exists.

Semiconductor bonding with Pyrex glass is a challenging technological issue. Currently, anodic bonding is used, but it leaves oxygen residues on the surface of the glass [16]. This issue has been addressed by prebaking the glass in a reducing atmosphere to remove the oxygen residues from the surface. This prebake treatment results in a strong and sharp bonded interface between glass and GaAs without the growth of nanostructures in the glass. The baking of the materials reduced the mobility of ions and restricted the growth of nanostructures [16]. Using photolithography [17] and nanoimprinting lithography [18], nanostructures can be fabricated on different substrates, but a void-free interface must be maintained to grow fine-pitch and well-controlled nanostructures. However, to the best of our knowledge, there is no technology that offers growth of GaAs nanostructures in glass. Therefore, a simple low-cost process to grow GaAs nanostructures in glass not only has scientific value, but it is also essential in systems integration using components from heterogeneous technologies such as electronics, photonics and fluidics.

Here, we propose a simple wafer-scale growth process using the hybrid plasma bonding (HPB) method in air. One measure of the efficacy of the proposed bonding process is the ability to grow nanostructures (of GaAs, for example) in glass through atomic adhesion at low temperatures. In this method, the surfaces are sequentially activated using an oxygen (O_2) reactive ion etching (RIE) plasma and nitrogen (N_2) microwave (MW) radicals. The plasma processing removes surface contaminations by the physical sputtering mechanism [19] and creates chemically reactive surfaces. Finally, the activated surfaces are contacted in air under an applied voltage at low temperature.

In our prior work, we achieved void-free silicon (Si)/Pyrex glass and germanium (Ge)/Pyrex glass interfaces with high bonding strength (∼18 MPa) [14, 19]. The strong void-free, bonded interface met the prerequisite for the growth of nanostructures, but no growth of Si and Ge nanostructures was observed in glass. We observed that glass neither receives ions from nor donates them to the anode in HPB. Rather, it shares negative ions that form oxides at the wafer on the anode [14, 19]. The HPB approach for Pyrex and GaAs enables the negative ions of glass to flow toward GaAs and an equivalent amount of Ga and As ions toward glass under thermally-induced electrostatic forces and an applied voltage. Therefore, the simple low-cost formation and manipulation of GaAs nanostructures over a wide area of Pyrex glass is the key outcome in hybrid plasma bonding.

In this paper, we describe a simple low-cost growth process for GaAs nanostructures in Pyrex glass using the hybrid plasma bonding method. We investigate the chemical compositions of the surfaces to illustrate the growth mechanism of the nanostructures. Finally, we study the cross-section of the bonded interface to characterize the GaAs nanostructures and discuss their growth mechanism.

2. Growth and characterization techniques

Commercially available 100 mm diameter Pyrex glass and p-type 50 mm size GaAs wafers with mirror polished surfaces were used for HPB to grow GaAs nanostructures in the glass. The Pyrex glass contained 81%-SiO_2, 13%-B_2O_3, 4%-Na_2O and 2%-Al_2O_3.

We have used GaAs and glass wafers as received. We have neither polished nor dipped the wafers in wet chemicals and/or water. Table 1 summarizes the characteristics of the wafer surfaces and the plasma processing parameters for the growth. These are the optimized parameters obtained from our published results of HPB in Si/glass [20] and Ge/glass [14]. Interested readers can refer to [20, 14] for more parameterizations of the growth. The surfaces were sequentially activated using a 50 W oxygen (O_2) radio frequency (RF) reactive ion etching (RIE) plasma at a frequency of 13.56 MHz for 15 s at 60 Pa followed by a 2500 W microwave (MW) nitrogen (N_2) radicals at a frequency of 2.45 GHz for 30 s at 60 Pa. The background vacuum pressure in the plasma activation chamber was 10^{-1} Pa. The activated surfaces were contacted under hand-applied pressure outside the vacuum chamber in the clean room and cold rolled under 0.2 MPa pressure by a cold roller in order to remove any air trapped at the interface. Finally, the contacted wafers were treated at 200 °C under an

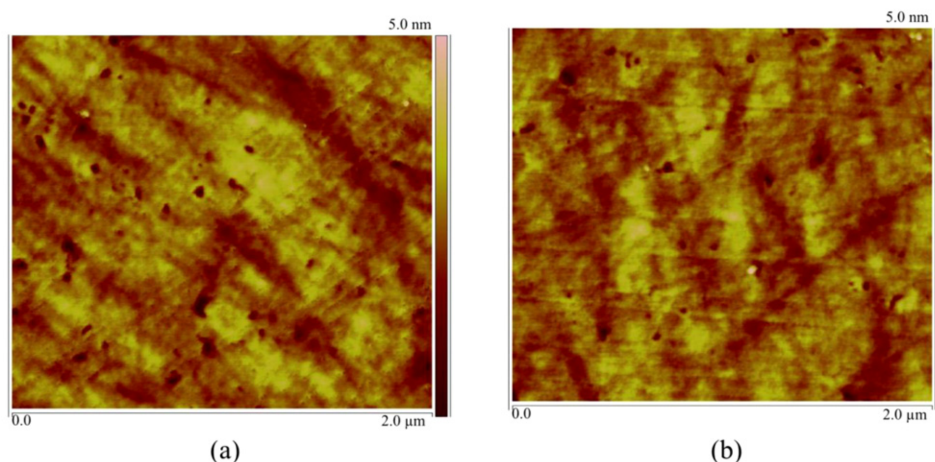

Figure 1. AFM images of glass (a) before plasma activation, (b) after sequential plasma activation.

applied voltage of 1 kV for 10 min and an external pressure of 0.07 MPa in the anodic bonding chamber. The processing time to grow the GaAs nanostructures in the Pyrex glass was less than 30 min.

It was found that strong adhesion and smooth surfaces are required for the growth of GaAs nanostructures. The growth was evaluated in terms of the surface energy, using a Kruss Drop Shape Analysis system DSA100, and the surface quality, using a Veeco atomic force microscope. A silicon tip in tapping mode was utilized for the surface roughness measurement over a scanning area of 2 μm × 2 μm. To illustrate the growth mechanism of the nanostructures, the chemical compositions of complex bonded atoms at the surface before and after plasma cleaning were observed using a Renishaw Raman spectrometer with 514 and 785 nm lasers. To characterize the structural and elemental compositions of the GaAs nanostructure growth in the glass, high-resolution transmission electron microscopy (HRTEM) and scanning transmission electron microscopy (STEM) were used.

3. Results and discussion

3.1. Surface roughness and adhesion

We have observed that the root mean square (RMS) surface roughness of glass is higher than that of GaAs. The high surface roughness is due to the defects and scratches left on the glass surface after chemical–mechanical planarization (CMP). Some of these defects are of nm-size and both defects and scratches are the result of inhomogeneous interactions of alkaline and silicate elements of glass with the CMP slurry (see figure 1(a)) [1]. It was found that the surface roughness improved after surface activation (table 1 and figure 1(b)). Values of surface roughness, water contact angle, and bonding parameters are presented in table 1.

For GaAs and glass, their surface energy is an important parameter because it controls the bond strength across the GaAs–glass interface. A measure of the surface energy is its water contact angle. A lower water contact angle indicates a higher surface hydrophilicity, which is desirable for a stronger bonded interface. This can be explained from Young's equation in equilibrium [21], which relates surface hydrophilicity to surface energy. Our results of lower water contact angles of GaAs and glass indicate higher surface energies and, therefore, a higher bonding strength of the interface.

Figure 2 shows optical images of GaAs/glass using anodic bonding (figure 2(a)) and HPB (figure 2(b)). The anodically bonded wafers were fractured due to the mismatch in the coefficient of thermal expansion between GaAs and glass, which caused delamination. Therefore, we use HPB to bond GaAs with Pyrex. However, with HPB, the bonded interface exhibited a large void which was due to the presence of contaminants on the activated surface and the entrapment of air. With HPB, the GaAs/glass had a high tensile strength of 7.2 ± 0.7 MPa. Also, using HPB, it was found that the pore size controls the size of the nanostructures. To control the pore size, we can vary the plasma energy. In our earlier study [22], plasma induced defect sites such as nanopores and craters were observed on Si surfaces that were treated with a relatively high energy (i.e., 400 W) of O_2 RIE plasma. Furthermore, the density and sites of the nanostructures may be controlled through the placement of nanopores. In addition, the electrostatic force in the anodic step of HPB can be used to control the length of the nanostructures. Recently, we have observed that the influence of the electrostatic force on the depletion layer of Si/glass and Ge/glass was significantly different [14, 20]. While the interface of Si/glass had an alkaline depletion layer with a thickness of 353 nm in the glass, the depletion layer of Ge/glass was about a micrometer. Since the experimental conditions that induce electrostatic force (i.e., anodic voltage and temperature) Si/glass and Ge/glass bonding were identical, different thicknesses of the depletion layers indicate that the electrostatic force controls the height of the growth layer.

3.2. Raman spectroscopy of GaAs surface

GaAs is a sensitive material in which Ga and As react readily with air and produces unstable native oxides. Also,

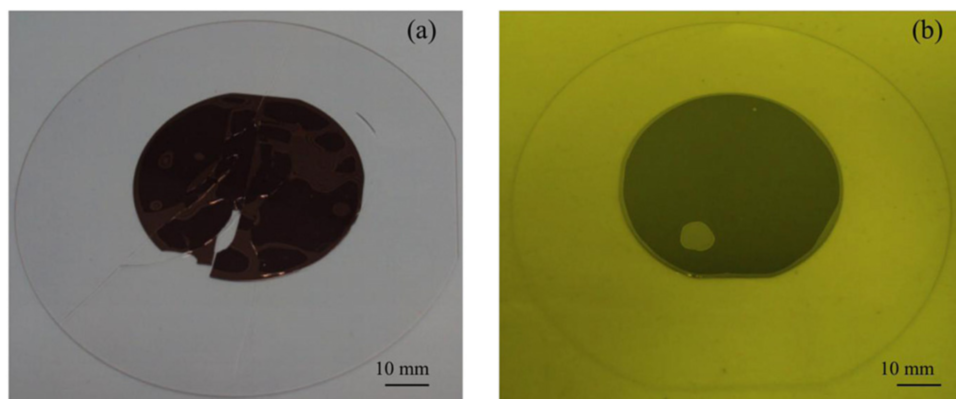

Figure 2. Optical images of GaAs/glass bonded interfaces at 200 °C with a 1 kV voltage for 10 min using (a) anodic bonding and (b) sequential plasma activation followed by anodic bonding (HPB).

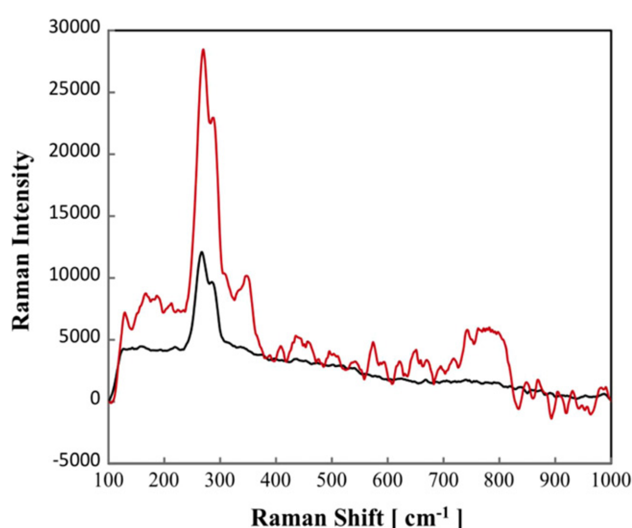

Figure 3. Raman spectra of GaAs before and after activation. Note that the black and red curves indicate the spectra before and after activation.

oxygen diffusion and drifting of Ga and As under oxygen plasma treatment have been reported in [23]. To study the molecular and crystal lattice vibrations, surface compositions, chemical environment, bonding and structure of the GaAs surface [24], Raman spectroscopy was used. Figure 3 shows the Raman bands of 'as received' GaAs samples before and after the sequential plasma activation. Major peaks in the range 200–400 cm^{-1} before and after activation are shown.

From the Raman spectrum, a multiple Gaussian fit was used to assist in identifying the chemical species. The peaks of the deconvolved spectra with identification are shown in table 2. Before activation, the four peaks (figure 3 and table 2) of GaAs, the native oxide of GaAs (Ga–As–O), the longitudinal optical (LO) phonon mode of GaAs, and Ga_2O_3 are observed. It is noted that the native oxide of GaAs forms a metastable Ga–O–As complex [25] due to the decreased ratio of oxidized As:Ga at the surface with the increase of oxide thickness [25, 26]. The slow transport of arsenic through the growing oxide film, evaporation of arsenic oxide and the instability of arsenic oxide in the presence of GaAs resulted in the depletion of As [26]. Therefore, the Raman peak at 328.7 cm^{-1} can be assigned as a gallium oxide, Ga_2O_3, peak.

The sequentially treated GaAs showed four major peaks due to GaAs (TO), GaAs (LO), As_2O_5 and Ga_2O_3 (figure 3 and table 2). The peak before activation at 328.7 cm^{-1} (figure 3 and table 2) was shifted into a strong intense peak at 347.8 cm^{-1} after activation (figure 3 and table 2). The peak due to the native oxide of GaAs at 272.5 cm^{-1} (figure 3 and table 2) vanished after the activation. Instead of this peak, the strong peak at 347.8 cm^{-1} (figure 3 and table 2) was assigned as Ga_2O_3 due to the oxidation of GaAs in the O_2 RIE plasma [27, 23]. The formation of Ga_2O_3 (347.8 cm^{-1}) resulted from surface etching with plasma activation of GaAs, which depletes the volatile arsenic (interdiffusion with oxygen) and enriches the gallium [23, 28]. The O_2-RIE plasma activation significantly increases the absolute intensity of the chemical species due to the removal of carbon contamination and also results in GaAs surface oxidation [23, 28].

3.3. Raman spectroscopy of Pyrex glass surface

The behavior of alkaline contents and the three-dimensional network structure of Si and oxygen (i.e., Si–O–Si) in glass after surface activation is a key parameter for the growth of GaAs nanostructures. Before and after plasma activation, two bands at low frequencies between 200 and 600 cm^{-1} and at higher frequencies between 700 and 2100 cm^{-1} were observed. Also, a minor peak around 810–815 cm^{-1} (figure 4) was observed due to pyroborate units (i.e., B–O–B) (not shown in table 2) [29]. The intensity of the low frequency band is significantly weaker than that of the high frequency band. This weaker intensity indicates the influence of alkaline contents on the three-dimensional network structure of Si and oxygen (i.e., Si–O–Si) [30]. The shape of the spectra at the lower frequency indicates the inclusion of alkaline atoms, which may break the silicate network. At low frequencies, peaks were identified at 373.5, 455 and 488.4 cm^{-1} (figure 4 and table 2) due to the alkaline–oxygen–alkaline stretching, Si–O–Si networks and aluminate networks (Al–O/Al–O–B),

Table 2. Summary of deconvolved Raman spectra of GaAs and glass from figures 3 and 4 before and after surface activation.

Specimen	Range of wavenumbers (cm^{-1})	Peaks of deconvolved spectra				Identification of peaks
		Before activation		After activation		
GaAs	200–400	264.4	Figure 3	269.2	Figure 3	GaAs (TO)
		272.5		Disappear		Native oxide
		288.5		290.5		GaAs (LO)
		—		308.6		As_2O_5
		328.7		347.8		Ga_2O_3
Glass	200–600	373.5	Figure 4	379	Figure 4	Alkaline–oxygen–alkaline stretches
		455		457.8		Si–O–Si networks
		488.4		489.4		Al–O/Al–O–B networks
	700–2100	1288.2		1289		Adventitious carbon
		1437		1436.3		Boroxol chain and ring
		1558.9		1557.2		Amorphous carbon
		1749.7		1767		Hydroxyl

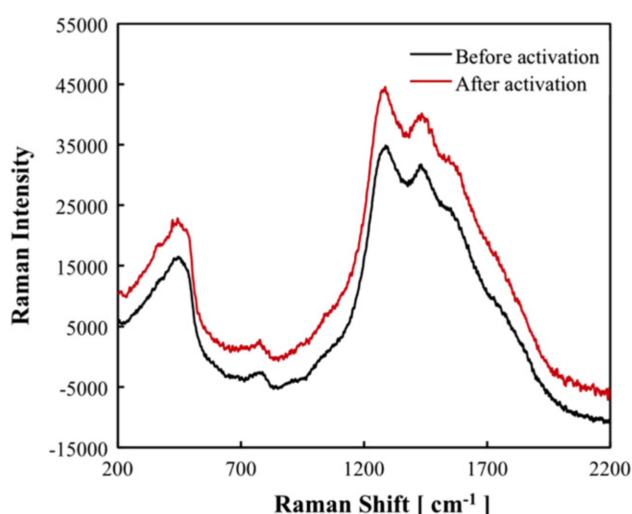

Figure 4. Raman spectra of glass before and after activation.

respectively. The shapes are very similar to those before activation. Also, the higher wavenumbers from the glass surface after activation are due to the additional oxygen passivation.

Before activation, in the high frequency band, four peaks (table 2) were observed due to the adventitious amorphous carbons (1288.2 and 1558.9 cm^{-1}), boroxol chain and ring (B–O–) (1437 cm^{-1}), and hydroxyl stretch (1749.7 cm^{-1}) [29–33]. The first three peaks were not shifted after the sequential activation, but the last one was shifted from 1749.7 to 1767 cm^{-1} (table 2). This shift is due to the reaction of the oxygen from the O_2 RIE step in the activation process with silicon in the glass. Also, the amorphous carbon peak at 1437 cm^{-1} that remains after the plasma activation may be due to the low power of O_2 RIE and low background vacuum pressure. The passivated films before and after sequential plasma treatment may suppress the non-bridging oxygen atoms (850–1250 cm^{-1}).

3.4. Observation of GaAs nanostructure growth

Figure 5 shows the HRTEM (figure 5(a)) and STEM (figure 5(b)) images of GaAs nanostructures growth in Pyrex glass. The bonded interface of GaAs/glass shows two amorphous layers and a crystalline lattice layer (figures 5(a) and (b)). The interfacial morphology observed by the high angle annular dark field (HAADF)-STEM was identical to that in the HRTEM images. Sharp contrasts between the crystalline lattice sites and the amorphous GaAs and between the amorphous GaAs and amorphous glass were observed. The thickness of the amorphous GaAs layer varied from 3 to 10 nm due to plasma activation damage induced in the single-crystal GaAs. The inhomogeneity in the thickness of the GaAs amorphous layers could be attributed to the variation of the elemental flow of GaAs into glass during HPB.

The height of the GaAs nanostructures varied from 30 to 50 nm (figure 5(b)). This is in contrast to the penetration depth of Ga into the glass, which has been theoretically calculated to be in the nanometer range (∼4 nm) [16]. However, the individual nanostructures at various locations had a similar morphology. The growth of nanostructures maintained a regular pattern with heights ranging from 20 to 50 nm. This indicates that GaAs is an anodic material with a partially blocking nature [34]. The growth of nanostructures from GaAs to glass indicates the pulling of Ga and As ions into the glass. It is expected that manipulation of glass impurities and surface morphology will permit control of the nanopore location.

3.5. Elemental detection of GaAs nanostructures

Energy dispersive x-ray (EDX) spectroscopy analysis confirms GaAs nanostructures in the glass. Figure 6(a) shows the quantitative analysis of the elemental composition ‘on nanostructures’ compared with that ‘off nanostructures’ (i.e., bulk area) of the glass. The red curve shows the elements on nanostructures. The black curve represents elements outside of the nanostructures. On the nanostructures, both Ga and As were observed. Off the nanostructures, Si and O, which are the major elements in the glass, were observed. Carbon elements on both ‘on’- and ‘off’-nanostructures were observed due to the contamination from HRTEM.

Figure 6(b) shows the distribution of oxygen, silicon, gallium and arsenic across the bonded interface. The EDX

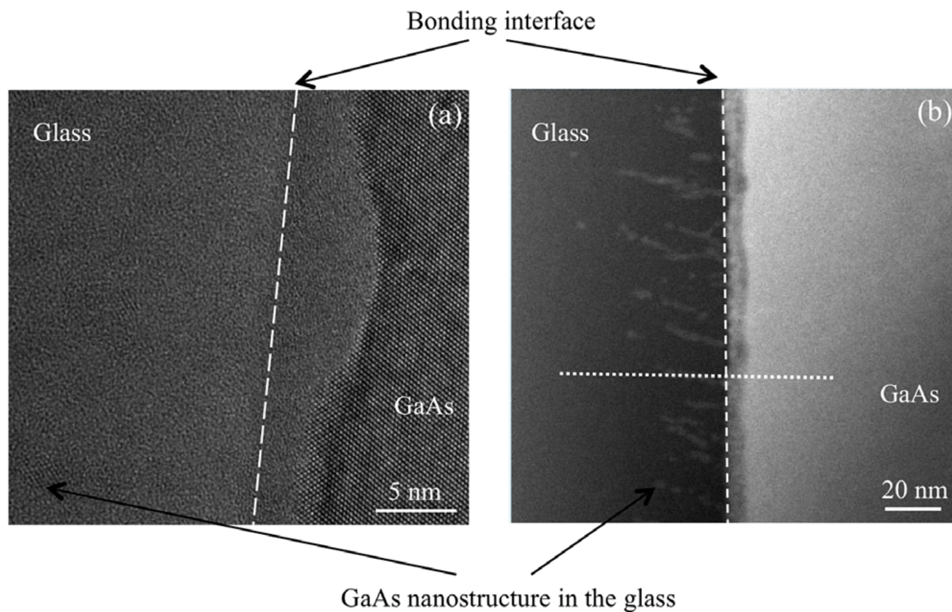

Figure 5. (a) HRTEM and (b) STEM images of the hybrid plasma bonded GaAs/glass interface. Here, GaAs and glass amorphous layers across the interface and GaAs nanostructures in glass are observed.

scan line position was 'on nanostructures', as shown in figure 5(b). It is seen that gallium and arsenic diffused into the glass. A certain amount of oxygen was observed on GaAs across the bonded interface due to the electrostatic force induced by the high voltage and temperature during anodic bonding. Under these circumstances, GaAs could be decomposed. Therefore, the nanostructures were grown due to the exchange between the negative ions of glass toward GaAs and an equivalent amount of Ga and As toward the glass.

3.6. Growth mechanism of GaAs nanostructures

From the Raman spectra results, Pyrex glass containing alkaline oxide compounds such as boroxol chains may be broken during bonding under the electrostatic force due to the application of an anodic voltage and heating [35]. The alkaline atoms resulting from the broken alkaline oxide compounds flow toward the cathode. A driving force is required to maintain the flow of alkaline atoms and the amount of Ga and As must be equivalent to the alkaline ions. In order to fill the vacancies of alkaline atoms, Ga ions followed by As ions flow to the glass. The movement of gallium ions is controlled by diffusion and by drift in the electric field at high temperature [16, 35]. The electrostatic fields are non-uniformly distributed over the plasma-activated rough surface of glass at the interface due to the presence of nanodefects and nanopores during anodic bonding. This nonlinear behavior of the electrostatic force results in a higher electric field at the nanopores (due to the thicker oxide) than in other areas. Therefore, Ga ions move easily into glass through the nanopores at the interface. In addition, the partially blocking nature [34] of GaAs during bonding with the Pyrex glass is attributed to the inhomogeneous growth of GaAs nanostructures in the glass. Therefore, the pulling of Ga and As ions from GaAs to glass due to the movement of alkaline ions under the high electrostatic forces resulted in the growth of GaAs nanostructures in the glass.

Recently, the role of silicon nitride (Si_xN_y) nanomasks on the defect densities and structural properties of heteroepitaxially grown gallium nitride (GaN) nanocrystallites on sapphire has been investigated [36]. Two sets of specimens of GaN with heavily doped Si with densities of 2×10^{20} cm^{-3} were used. The nanogrowth was characterized with and without inserting Si_xN_y nanomasks at the interface between the GaN seed layer and the GaN main layer (heavily doped). The specimen without Si_xN_y resulted in GaN crystallites a few hundred nm length with considerably reduced defect densities. The structural properties of the growth crystallites of the specimens with and without Si_xN_y were different. In another study [37], the formation of defects across grains in the aluminum doped zinc oxide films favored the growth. Therefore, the surface and interfacial defects control the growth behaviors of the oxide and nitride nanocrystallites in these studies. These behaviors are similar to that of the observed non-trivial growth behavior of GaAs nanostructures in Pyrex through defects such as pores and scratches.

In this study, the nanostructures were grown at the locations of pores and scratches on the glass surface. Precise positioning of nanopores and nanolines is required to achieve their controlled size and pitch. These nanopores and nanolines may result in nanowires and nanosheets, respectively. A variety of methods, such as focused ion beam [38], interference lithography [39], electron beam lithography [38] and nanoimprinting lithography [40, 17] can be used to create nanopores and nanolines at desired locations. For the length manipulation of the grown nanostructures, the electrostatic force can be controlled during the anodic step in the HPB. The electrostatic force is known to be a function of the applied electrical field, temperature and time [15, 30, 31].

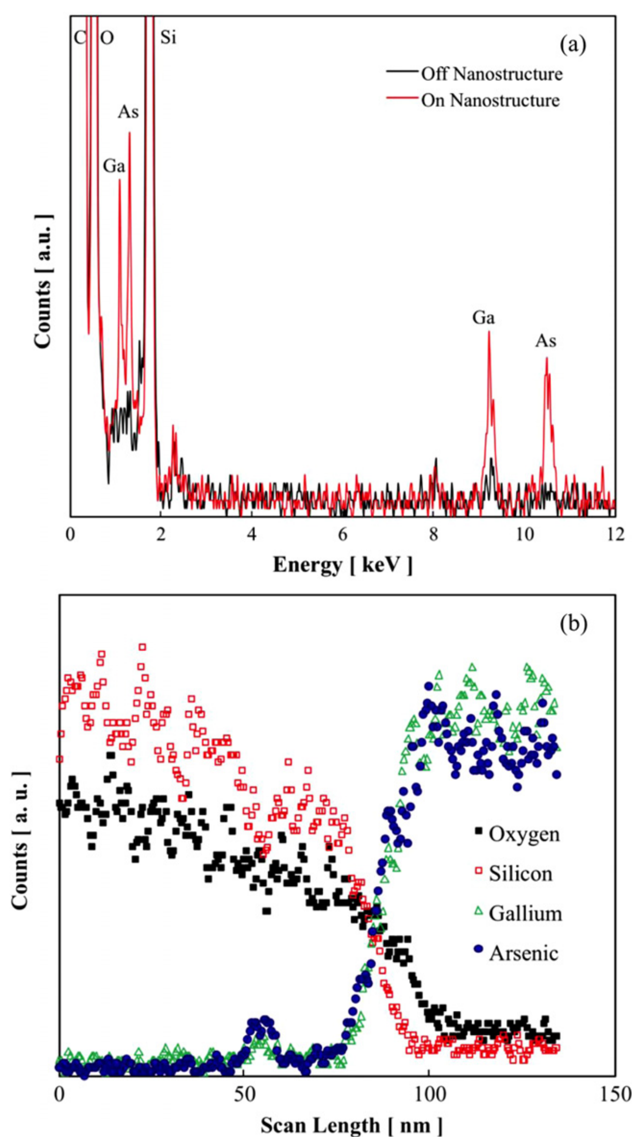

Figure 6. (a) Energy dispersive x-ray (EDX) spectra of the elemental intensity of C, O, Si, Ga and As at 'Off Nanostructure' and 'On Nanostructure'. (b) EDX spectra of elemental distribution at 'On Nanostructure' across the bonded interface. The scan position on nanostructure is indicated by a dotted line, as shown in figure 5(b).

The controlled growth of GaAs nanostructures in Pyrex glass may offer a unique opportunity to realize a low-cost fluidic filtration system [41, 42, 2, 43].

4. Conclusions

Gallium arsenide nanostructures were grown, for the first time in glass, using the hybrid plasma bonding (HPB) in air between the smooth surfaces of GaAs and glass substrates. HPB is observed to assist the migration of ions to achieve the void-free bonded interface that is necessary for our nanostructure growth. The atomic level bonding of GaAs/glass and inhomogeneous growth of GaAs nanostructures in glass were confirmed by high-resolution transmission electron microscopy and high angle annular dark field-scanning tunneling electron microscopy. This inhomogeneous growth was attributed to the partially blocking effect of GaAs associated with the nanostructures in the glass. Energy dispersive x-ray (EDX) analysis showed the flow of alkaline ions toward the cathode and replacement of alkaline ions by Ga and As ions in glass. EDX detected both Ga and As on the grown nanostructures. The Raman observation showed the alkaline contents on the three-dimensional network structure of Si and oxygen, and the boroxol chain in the Pyrex glass, and identified oxidized GaAs after plasma activation. During the anodic bonding, the alkaline ions moved toward the cathode and were substituted by Ga and As ions. The electrostatic force induced by the applied electrical field and heating in the anodic step of the bonding controls the length of the nanostructures. Through control of the GaAs nanostructure growth location by nanopores, nanolines and density on Pyrex glass, a low-cost fluidic filtration system may be realized.

Acknowledgments

This research is supported by discovery grants from the Natural Science and Engineering Research Council of Canada, an infrastructure grant from the Canada Foundation for Innovation (CFI) and an Ontario Research Fund for Research Excellence Funding Grant. The authors gratefully acknowledge Professor Tadatomo Suga, University of Tokyo for his continuous support and Professor Alex Adronov, Professor Peter Kruse, and Steve Kornic, McMaster University for their assistance in the Raman experiments. Arif Ul Alam is acknowledged for his help in the preparation of the manuscript. The Canada Center for Electron Microscopy (CCEM) at McMaster University is also acknowledged for the HRTEM experiments. One author (MJD) also expresses his thanks to the ITCE Division, POSTECH for hosting him as a Distinguished Visiting Professor through the S Korean Ministry of Education, Science, and Technology Program (project R31-2008-000-10100-0), during the final preparations of the manuscript.

References

[1] Iliescu C, Miao J and Tay F E H 2005 Stress control in masking layers for deep wet micromachining of Pyrex glass *Sensors Actuators* A **117** 286–92
[2] Wei Hou H, Gan H Y, Bhagat A A S, Li L D, Lim C T and Han J 2012 A microfluidics approach towards high-throughput pathogen removal from blood using margination *Biomicrofluidics* **6** 024115
[3] Howlader M M R, Suehara S and Suga T 2006 Room temperature wafer level glass/glass bonding *Sensors Actuators* A **127** 31–6
[4] Lin W-Y, Wang Y, Wang S and Tseng H-R 2009 Integrated microfluidic reactors *Nano Today* **4** 470–81
[5] Fokine M 2009 Manipulating glass for photonics *Phys. Status Solidi* a **206** 880–4
[6] Deen M J, Shinwari M W, Ranuárez J C and Landheer D 2006 Noise considerations in field-effect biosensors *J. Appl. Phys.* **100** 074703
[7] Howlader M M R, Selvaganapathy P R, Deen M J and Suga T 2011 Nanobonding technology toward electronic, fluidic,

and photonic systems integration *IEEE J. Sel. Top. Quantum Electron.* **17** 689–703

[8] Howlader M M R, Suehara S, Takagi H, Kim T H, Maeda R and Suga T 2006 Room-temperature microfluidics packaging using sequential plasma activation process *IEEE Trans. Adv. Packag.* **29** 448–56

[9] Deen M J and Basu P K 2012 *Silicon Photonics—Fundamentals and Devices* (New York: Wiley) pp 1–12

[10] Wang D-S, Chao J-J, Hung S-C and Lin C-F 2009 Fabrication of large-area gallium arsenide nanowires using silicon dioxide nanoparticle mask *J. Vac. Sci. Technol.* B **27** 2449

[11] Aravamudhan S, Ramgir N and Bhansali S 2007 Electrochemical biosensor for targeted detection in blood using aligned Au nanowires *Sensors Actuators* B **127** 29–35

[12] Pi X D 2004 Characterization of the interface region during the agglomeration of silicon nanocrystals in silicon dioxide *J. Appl. Phys.* **95** 8155

[13] He Y, Fan C and Lee S-T 2010 Silicon nanostructures for bioapplications *Nano Today* **5** 282–95

[14] Howlader M M R, Kibria M G and Zhang F 2010 Hybrid plasma bonding of germanium and glass wafers at low temperature *Mater. Lett.* **64** 1532–5

[15] Ohira K, Kobayashi K, Iizuka N, Yoshida H, Ezaki M, Uemura H, Kojima A, Nakamura K, Furuyama H and Shibata H 2010 On-chip optical interconnection by using integrated III–V laser diode and photodetector with silicon waveguide *Opt. Express* **18** 15440–7

[16] Hok B, Dubon C and Ovren C 1983 Anodic bonding of gallium arsenide to glass *Appl. Phys. Lett.* **43** 267–9

[17] Sun Y, Khang D-Y, Hua F, Hurley K, Nuzzo R G and Rogers J A 2005 Photolithographic route to the fabrication of micro/nanowires of III–V semiconductors *Adv. Funct. Mater.* **15** 30–40

[18] Yao J, Le A-P, Gray S K, Moore J S, Rogers J A and Nuzzo R G 2010 Functional nanostructured plasmonic materials *Adv. Mater.* **22** 1102–10

[19] Deen M 1987 The effect of the deposition rate on the properties of dc-magnetron-sputtered niobium nitride thin films *Thin Solid Films* **152** 535–44

[20] Howlader M M R, Kibria M G, Zhang F and Kim M J 2010 Hybrid plasma bonding for void-free strong bonded interface of silicon/glass at 200 degrees C *Talanta* **82** 508–15

[21] Ma X, Chen C, Liu W, Liu X, Du X, Song Z and Lin C 2009 Study of the Ge wafer surface hydrophilicity after low-temperature plasma activation *J. Electrochem. Soc.* **156** H307

[22] Howlader M M R, Zhang F and Kibria M G 2010 Void nucleation at a sequentially plasma-activated silicon/silicon bonded interface *J. Micromech. Microeng.* **20** 065012

[23] Grigonis A, Galdikas A and Silinskas M 1999 The oxidation of surface layers during reactive ion etching of GaAs in $CF_2Cl_2 + O_2$ and O_2 plasmas *Appl. Surf. Sci.* **138/139** 581–6

[24] Spirkoska D, Abstreiter G and Fontcuberta I Morral A 2008 Size and environment dependence of surface phonon modes of gallium arsenide nanowires as measured by Raman spectroscopy *Nanotechnology* **19** 435704

[25] Mizokawa Y, Komoda O and Miyase S 1988 Long-time air oxidation and oxide-substrate reactions on GaSb, GaAs and GaP at room temperature studied by x-ray photoelectron spectroscopy *Thin Solid Films* **156** 127–43

[26] Grunthaner P J 1980 Chemical depth profiles of the GaAs/native oxide interface *J. Vac. Sci. Technol.* **17** 1045

[27] Chang R P H 1979 Some properties of plasma-grown GaAs oxides *Thin Solid Films* **56** 89–106

[28] Howlader M M R, Suga T, Zhang F, Lee T H and Kim M J 2010 Interfacial behavior of surface activated p-GaP/n-GaAs bonded wafers at room temperature *Electrochem. Solid-State Lett.* **13** H61

[29] Li H, Su Y, Li L and Strachan D M 2001 Raman spectroscopic study of gadolinium(III) in sodium–aluminoborosilicate glasses *J. Non-Cryst. Solids* **292** 167–76

[30] Matson D W, Sharma S K and Phillpotts J A 1983 The structure of high-silica alkali-silicate glasses. A Raman spectroscopic investigation *J. Non-Cryst. Solids* **58** 323–52

[31] Santra T S, Liu C H, Bhattacharyya T K, Patel P and Barik T K 2010 Characterization of diamond-like nanocomposite thin films grown by plasma enhanced chemical vapor deposition *J. Appl. Phys.* **107** 124320

[32] McMillan P and Remmele R L Jr 1986 Hydroxyl sites in SiO_2 glass: a note on infrared and Raman spectra *Am. Miner.* **71** 772–8

[33] De Bonfils J, Peuget S, Panczer G, De Ligny D, Henry S, Noël P-Y, Chenet A and Champagnon B 2010 Effect of chemical composition on borosilicate glass behavior under irradiation *J. Non-Cryst. Solids* **356** 388–93

[34] Carlson D E, Hang K W and Stockdale G F 1972 Alkali-containing glasses *J. Am. Ceram. Soc.* **1971** 337–41

[35] Van Helvoort A T J, Knowles K M and Fernie J A 2003 Nanostructures at electrostatic bond interfaces *J. Am. Ceram. Soc.* **86** 1773–6

[36] Wieneke M, Noltemeyer M, Bastek B, Rohrbeck A, Witte H, Veit P, Bläsing J, Dadgar A, Christen J and Krost A 2011 Heavy Si doping: the key in heteroepitaxial growth of a-plane GaN without basal plane stacking faults? *Phys. Status Solidi* b **248** 578–82

[37] Koidis C, Logothetidis S, Kassavetis S, Laskarakis A, Hastas N A and Valassiades O 2010 Growth mechanisms and thickness effect on the properties of Al-doped ZnO thin films grown on polymeric substrates *Phys. Status Solidi* a **207** 1581–5

[38] Lo C J, Aref T and Bezryadin A 2006 Fabrication of symmetric sub-5 nm nanopores using focused ion and electron beams *Nanotechnology* **17** 3264–7

[39] Du K, Wathuthanthri I, Mao W, Xu W and Choi C-H 2011 Large-area pattern transfer of metallic nanostructures on glass substrates via interference lithography *Nanotechnology* **22** 285306

[40] Wu M-Y, Smeets R M M, Zandbergen M, Ziese U, Krapf D, Batson P E, Dekker N H, Dekker C and Zandbergen H W 2009 Control of shape and material composition of solid-state nanopores *Nano Lett.* **9** 479–84

[41] Nakashima Y, Hata S and Yasuda T 2010 Blood plasma separation and extraction from a minute amount of blood using dielectrophoretic and capillary forces *Sensors Actuators* B **145** 561–9

[42] Tey J N, Wijaya I P M, Wei J, Rodriguez I and Mhaisalkar S G 2010 Nanotubes-/nanowires-based, microfluidic-integrated transistors for detecting biomolecules *Microfluidics Nanofluidics* **9** 1185–214

[43] Hou H W, Bhagat A A S, Lee W C, Huang S, Han J and Lim C T 2011 Microfluidic devices for blood fractionation *Micromachines* **2** 319–43